

OCEAN CURRENT AND SEA ICE STATISTICS FOR DAVIS STRAIT

Y. Wu, C.G. Hannah, B. Petrie, R. Pettipas, I. Peterson, S. Prinsenber,
C. M. Lee and R. Moritz

Ocean and Ecosystem Sciences Division
Maritimes Region
Fisheries and Oceans Canada

Bedford Institute of Oceanography
P.O. Box 1006
Dartmouth, Nova Scotia
Canada B2Y 4A2

2013

**Canadian Technical Report of
Hydrography and Ocean Sciences 284**



Fisheries and Oceans
Canada

Pêches et Océans
Canada

Canada

**Canadian Technical Report of
Hydrography and Ocean Sciences 284**

2013

Ocean current and sea ice statistics for Davis Strait

by

Y. Wu, C.G. Hannah, B. Petrie, R. Pettipas, I. Peterson, S. Prinsenber,
C. M. Lee¹ and R.Moritz¹

Ocean and Ecosystem Sciences Division
Fisheries and Oceans Canada
Bedford Institute of Oceanography
P.O. Box 1006
Dartmouth, Nova Scotia
Canada B2Y 4A2

¹ Applied Physics Laboratory, University of Washington 1013 NE 40th Street Box
355640 Seattle, WA98105-6698, USA

©Her Majesty the Queen in Right of Canada, 2013

Cat. No. Fs 97-18/284E ISSN 0711-6764

Correct Citation for this publication:

Wu, Y., C.G. Hannah, B. Petrie, R. Pettipas, I. Peterson, S. Prinsenberg, C. M. Lee and R. Moritz. 2013. Ocean current and sea ice statistics for Davis Strait. Can. Tech. Rep. Hydrogr. Ocean Sci. 284: vi + 47p.

TABLE OF CONTENTS

TABLE OF CONTENTS.....	iii
LIST OF TABLES.....	iv
LIST OF FIGURES.....	v
ABSTRACT.....	vi
RÉSUMÉ.....	vi
1.0 INTRODUCTION.....	1
2.0 BACKGROUND OF CIRCULATION AND SEA ICE	
ACROSS DAVIS STRAIT.....	1
3.0 CURRENT DATA AND PROCESSING.....	2
3.1 NON-TIDAL CURRENTS.....	3
3.2 TIDAL CURRENTS.....	4
4.0 MAXIMUM CURRENTS.....	5
5.0 EXTREME CURRENTS.....	5
5.1 METHOD.....	5
5.2 EXTREME CURRENTS.....	6
6.0 SEA-ICE DRAFT.....	7
7.0 CONCLUSIONS.....	8
8.0 ACKNOWLEDGEMENTS.....	9
9.0 REFERENCES.....	10

LIST OF TABLES

Table 1	Mooring information in 2004-2011.....	12
Table 2	Annual and seasonal velocity means at selected layers in 2004-2011.....	13
Table 3	Annual and seasonal velocity means at selected layers in 2004-2005.....	14
Table 4	Annual and seasonal velocity means at selected layers in 2005-2006.....	15
Table 5	Annual and seasonal velocity means at selected layers in 2006-2007.....	16
Table 6	Annual and seasonal velocity means at selected layers in 2007-2008.....	17
Table 7	Annual and seasonal velocity means at selected layers in 2008-2009.....	18
Table 8	Annual and seasonal velocity means at selected layers in 2009-2010.....	19
Table 9	Annual and seasonal velocity means at selected layers in 2010-2011.....	20
Table 10	Tidal constants for M_2 constituent at selected layers in 2004-2011.....	21
Table 11	Tidal constants for N_2 constituent at selected layers in 2004-2011.....	22
Table 12	Tidal constants for S_2 constituent at selected layers in 2004-2011.....	23
Table 13	Tidal constants for O_1 constituent at selected layers in 2004-2011.....	24
Table 14	Tidal constants for K_1 constituent at selected layers in 2004-2011.....	25
Table 15	Extreme speeds with 10- and 30- year return periods.....	26
Table 16	Distributions of ice draft over an entire year.....	27
Table 17	Distributions of ice draft in fall.....	27
Table 18	Distributions of ice draft in winter.....	28
Table 19	Distributions of ice draft in spring.....	28
Table 20	Distributions of ice draft in summer.....	29

LIST OF FIGURES

Figure 1	General circulation, mooring array and instrument locations.....	30
Figure 2	Time series of 80 m velocity at BI4 in 2005-2006.....	31
Figure 3	Time series of 50 m velocity at C3 in 2005-2006.....	32
Figure 4	Time series of 54 m velocity at WG1 in 2005-2006.....	33
Figure 5	Maximum speed in 2004-2010.....	34
Figure 6	Vertical profiles of the maximum tidal speed.....	34
Figure 7	Gumbel distributions BI4 (30 m), C3 (30 m) and WG1 (30 m).....	35
Figure 8	Extreme speeds for 10- and 30- year return periods.....	36
Figure 9	Extreme speeds at selected layers for 10-year return period.....	37
Figure 10	Extreme speeds at selected layers for 30-year return period.....	37
Figure 11	Extreme speed for 10-year return period using the simple superposition method.....	38
Figure 12	Extreme speeds at selected layers for 10- year return period using the direct superposition method.....	38
Figure 13	Extreme non-tidal speed for 10-year return period.....	39
Figure 14	Extreme non-tidal speeds at selected layers for 10- year return period.....	39
Figure 15	Time series of ice draft at C1 in 2005-2006.....	40
Figure 16	Time series of ice draft at C2 in 2006-2007.....	41
Figure 17	Time series of ice draft at C4 in 2006-2007.....	42
Figure 18	Time series of ice draft at C6 in 2006-2007.....	43
Figure 19	Time series of ice draft at C2 in 2007-2008.....	44
Figure 20	Time series of ice draft at C4 in 2007-2008.....	45
Figure 21	Ice draft frequency distributions at C2 for 2006-2007, and 2007-2008.....	46
Figure 22	Ice draft frequency distributions at C4 for 2006-2007 and 2007-2008.....	46
Figure 23	Ice draft frequency distributions at C1, C2, C4 and C6.....	47

Abstract

Wu, Y., C.G. Hannah, B. Petrie, R. Pettipas, I. Peterson, S. Prinsenberg, C. M. Lee and R. Moritz. 2013. Ocean current and sea ice statistics for Davis Strait. Can. Tech. Rep. Hydrogr. Ocean Sci. 284: vi + 47p.

Rising global temperature is expected to reduce sea ice cover making it easier to exploit oil and gas reservoirs in high latitude offshore waters. However, sea ice will continue to be a potential hazard, so reliable information on sea ice and currents for platform design and offshore operations remains an important requirement. Based on statistical analysis of multi-year records from instrumented moorings, ocean current and sea ice properties across Davis Strait are presented in this report. Currents exceeding 1.5 m s^{-1} are mainly limited to the coastal waters of Baffin Island and West Greenland. The analyses show that the extreme currents near the Baffin Island coast are as high as $1.9\text{-}2.6 \text{ m s}^{-1}$ with a return period of 10 years. On the West Greenland Shelf, the extreme current speeds are $1.5\text{-}1.9 \text{ m s}^{-1}$ for a return period of 10 years. The maximum currents across the Strait mostly occur in fall when the ocean is free of sea ice. Sea ice draft has two components: level ice from thermodynamic processes such as freezing; and, deformed ice due to dynamic processes such as rafting. Sea ice is generally dominated by first year ice in the Davis Strait area. The ice free time varies from 60 days on Baffin Island Shelf to 200 days on West Greenland Shelf. Sea ice near the Baffin Island coast is generally thicker than that farther offshore and is thicker in winter and spring and thinner or not present in summer and fall. Mean ice draft is $1.4 \text{ m} (\pm 1.9\text{m})$ on Baffin Island Shelf and $0.2 \text{ m} (\pm 0.4\text{m})$ on the West Greenland Shelf. The maximum draft is about 20 m.

Résumé

Wu, Y., C.G. Hannah, B. Petrie, R. Pettipas, I. Peterson, S. Prinsenberg, C. M. Lee et R. Moritz. 2013. Ocean current and sea ice statistics for Davis Strait. Rapp. tech. can. hydrogr. sci. océan. 284 : vi + 47 p.

L'augmentation de la température planétaire devrait réduire la couverture de glace de mer, ce qui faciliterait l'exploitation des réservoirs de gaz et de pétrole dans les eaux de mer ouverte de hautes latitudes. Toutefois, la glace de mer sera toujours un danger potentiel et, par conséquent, le maintien de données fiables sur la glace de mer et les courants pour la conception de plates-formes et les activités extracôtières demeure une exigence importante. Dans le présent rapport, on présente les courants océaniques et les propriétés de la glace de mer le long du détroit de Davis en fonction d'analyses statistiques de documents pluriannuels provenant d'amarrages équipés. Les courants dépassant $1,5 \text{ m s}^{-1}$ se limitent principalement aux eaux côtières de l'île de Baffin et de l'ouest du Groenland. Les analyses révèlent que les courants très forts près de la côte de l'île de Baffin atteignent jusqu'à $1,9$ à $2,6 \text{ m s}^{-1}$ à une période de récurrence de 10 ans. Pour ce

qui est du plateau de l'ouest du Groenland, la vitesse des courants très forts est de 1,5 à 1,9 m s⁻¹ à une période de récurrence de 10 ans. Le long du détroit, les courants sont à leur vitesse maximale principalement à l'automne, période à laquelle il n'y a pas de glace de mer sur l'océan. Le tirant d'eau glacial de mer comprend deux éléments : la glace plane issue de processus thermodynamiques (p. ex. le gel) et la glace déformée provenant de processus dynamiques (p. ex. le chevauchement des glaces). Habituellement, la glace de mer est dominée par la glace de première année dans la région du détroit de Davis. La période où l'eau est libre de glace varie de 60 jours sur le plateau de l'île de Baffin à 200 jours sur le plateau de l'ouest du Groenland. Près de la côte de l'île de Baffin, la glace de mer est généralement plus épaisse que la glace située plus au large. Elle est d'ailleurs plus épaisse pendant l'hiver et le printemps et plus mince ou absente durant l'été et l'automne. Le tirant moyen de l'eau glacial est de 1,4 m ($\pm 1,9$ m) sur le plateau de l'île de Baffin et de 0,2 m ($\pm 0,4$ m) sur le plateau de l'ouest du Groenland. Par ailleurs, le tirant maximal est d'environ 20 m.

1.0 Introduction

A reduction in seasonal sea ice cover linked to rising global temperature is making it easier to drill and explore for oil and gas in high latitude offshore waters. Exploratory drilling in eastern Baffin Bay started in July 2010; more activity is planned in the next few years. Several lease blocks in deeper areas of Baffin Bay are being considered, and successful drilling there would increase interests in drilling in Canadian waters (<http://business.financialpost.com/2012/07/20/left-out-in-the-cold/?lsa=4c10-90c7>). Exploratory drilling in these ice infested waters requires high quality information on currents and sea ice to fulfill the requirement of the Canadian offshore operation regulation codes and provide key parameters for the safe design of platforms and rigs, and for their maintenance. To address these issues, results from the analysis of multi-year observations of ocean current and sea-ice draft data are presented here, with the principal products being extreme current speeds and mean and maximum sea ice draft statistics across Davis Strait. We present a brief summary of the circulation and sea ice variations in section 2. Section 3 describes the data and methods. The maximum current speeds are presented in section 4 and the extreme currents are presented in section 5. Sea ice draft data are presented in section 6. In the final section, major results are summarized.

2.0 General circulation and sea ice across Davis Strait

Davis Strait is a 350 km wide strait that connects Baffin Bay to the Labrador Sea in the northwest arm of the North Atlantic Ocean and is a key circulation pathway in subarctic-Atlantic region (Fig 1a). Water flowing through the Strait consists of two well-known opposing currents. One is the southward flowing Baffin Island Current (BIC) on the western side of Davis Strait; the other is the northward flowing West Greenland Current (WGC) on the eastern side. The WGC has a shelf component and a stronger, jet-like flow over the West Greenland slope. The BIC is mainly fed by the cold, relatively fresh Arctic waters that enter northern Baffin Bay through Nares Strait, Jones and Lancaster Sounds (Tang et al. 2004; Cuny et al. 2005; Curry et al. 2011). The WGC consists of two parts: one is the fresher current over the continental shelf and is considered as a continuation of the flow from the East Greenland Current; the second is the relatively warm and salty component from the Irminger Sea flowing over the WG slope (Cuny et al. 2005). The Irminger Sea water circulates cyclonically around the northern Labrador Sea, constrained by the shallow sill (maximum depth ~640 m) at Davis Strait.

Sea ice affects the exchange between the ocean and the atmosphere. The presence of sea ice can reduce the atmosphere-ocean exchange of heat and momentum and thus affect the circulation in the upper layer and movement of sea ice on the surface. At the same time, the presence of ice, especially rafted ice and icebergs, poses a serious threat to safe navigation and offshore oil and gas activities. On average in Davis Strait, sea ice appears in the middle of

October, reaches maximum coverage in March, and then starts to decay in April (Crane, 1978; Canadian ice Service 2012). The sea ice generally advances from west to east in the growth phase, and retreats from east to west in the decay phase. The mean ice draft across the Strait is about 1.0 m. However, the maximum reaches as much as 20 m due to rafting of ice according to snap-shot observations from submarine sonar profiles taken in February 1967 (Wadhams et al. 1985). Tang et al. (2004) showed the annual cycle of ice thickness based on long-term measurements at Clyde River (70.47°N, 67.42°W), Baffin Island. On average ice cover begins in late October; ice thickness increases through the winter reaching a maximum of about 1.6 m near the end of May. Ice thickness and cover rapidly decrease to ice free conditions by late July-early August.

3.0 Data and methods

The ocean current data used in this report are from October 2004 to September 2011, collected as part of a long-term monitoring program in Davis Strait (<http://iop.apl.washington.edu/projects/ds/html/overview.html>). The program included 11 moorings, two on the narrow Baffin Island shelf, three on the west Greenland shelf and six in the deep, central Strait. The moorings were typically deployed in September or October and recovered and redeployed annually. The mooring array is shown in Figure 1B, C. Acoustic Doppler current profilers (ADCPs) were deployed at about 100 m and Aanderaa RCM8 current meters at about 250 m and 500 m mainly at the sites in the central Strait. Details of mooring deployments are given in Table 1. The ADCP vertical resolution was 4 m for all deployments; each ADCP record was binned every 4 m from 10 m to 100 m. The velocity was linearly interpolated between the ADCP at 100 m and the RCM8s, at 250 and 500 m, at 4 m intervals. The sampling times were 30 minutes for the ADCP and hourly for RCM8, which was further linearly interpolated into 30 minutes to match the ADCP data. In order to build long time series, the records from BI3 and BI4 were merged as “BI4” and WG3 and WG4 were merged as “WG3” (Table 1).

Time series of the moored data were decomposed into tidal and non-tidal (residual) components using T-Tide (Pawlowicz et al. 2002). Examples of the time series of velocity 2005-06 before and after the decomposition at three sites are plotted in Figures 2-4. The three sites, from west to east, are BI4, C3 and WG1, represent the currents for the Baffin Island coast, central Davis Strait and the West Greenland shelf. As can be seen in Figure 2, currents at BI4 are dominated by the north-south component (v) with the magnitude reaching $\sim 1.0 \text{ m s}^{-1}$, which is 3-4 times stronger than that of the east/west component (u). For the north/south component, further examination indicates that the southward currents are stronger than the northward ones. During the observation period, high speeds mainly occur in the late fall and early winter

(November, December and January). Time series of tidal currents show that the speed in June and December reaches 0.75 m s^{-1} , slightly higher than March and September by 0.2 m s^{-1} (Fig. 2D). At this site, the magnitude of tidal currents exceeds that of residual currents (Fig. 2E). At mooring C3 in the central Strait, there is still a tendency for the v component to be stronger to the south (Fig. 3). Compared to BI4, magnitudes of both the residual and the tidal currents at C3 are weaker. The magnitude of the tidal speed is on average comparable to that of the residual speed. At WG1 on the outer edge of the West Greenland shelf, the magnitude of the east/west current is comparable to that of the north/south current, which is dominated by northward flows (Fig. 4). The high speed currents occur in fall and early spring. Tidal and residual flows are comparable to those at C3.

3.1 Non-tidal currents

For the non-tidal currents, the annual and seasonal means and standard deviations are estimated for the entire record 2004~2011 and for the seven specific mooring periods (see Table 1), respectively. The results for 2004-2011 are listed in Table 2, and the results in the specific years are listed in the Tables 3-9.

For the period of 2004-2011, the currents at the 9 mooring sites have strong seasonal and spatial variability. Across Davis Strait, the current shows a bimodal structure with southward flow, the dominant Baffin Island Current (BIC), from BI4 to C4, and the northward West Greenland Current (WGC) from C5 to WG3. For BIC, two cores are evident. One is at BI4, the Baffin Island Coastal Current, and the other is at C2, the Baffin Island Offshore Current. The magnitudes of the currents in the two cores in summer and fall are stronger than those in winter and spring. The first core at BI4 has a higher southward velocity, but lower eastward velocity than that of the second. For the WGC, the core of the current is found at C6. Similarly, the currents in summer and fall are stronger than those in winter and spring, when the ocean is usually covered by sea ice. Currents at all the mooring sites decrease from the surface except at C5 and C6, where the currents in the deep layer (100-500) are clearly stronger than those in the surface layer (<100 m) in winter and spring. Compared to the BIC (BI4-C4), the vertical distribution of the velocity of the WGC is more uniform.

Besides the mean values of the velocity, the standard deviations (STD) of u and v at each site are listed in Table 2 as well. This allows us to estimate the coefficients of variability of u and v by calculating the ratio of STD to the magnitudes of their corresponding means. Higher levels of the ratios indicate stronger variability and/or relatively weaker mean currents. The distribution of the ratios (not shown) has a strong spatial variation, both in u and v . For velocity u , ratios in the coastal areas (BI4, C1 and WG1) are generally larger than those in deep waters (C2, C3 and C4). For velocity v on the other hand, the ratios in the coastal areas are generally smaller than those in deep water. These spatial features of the velocity variability can also be found for the seasonal data, but with different intensities.

3.2 Tidal currents

The ellipse parameters of the five largest tidal constituents (M_2 , N_2 , S_2 , K_1 and O_1) for the entire record and selected depth layers are listed in Tables 10-14. To calculate these parameters, the time series of velocity within the given layer are firstly averaged and the parameters are then estimated with T_Tide. The ellipse parameters include the semi-major axis, semi-minor axis, inclination (measured counter-clockwise from east) and phase. In the following discussion, the focus is on the amplitude of the semi-major axis.

At BI4, the strongest tide is K_1 with a current magnitude of 0.27 m s^{-1} , which is higher than the magnitude of M_2 by 0.07 m s^{-1} . The O_1 current is about 0.09 m s^{-1} , and it is comparable to that of S_2 . The magnitude of N_2 is about 0.06 m s^{-1} , weaker than the other four constituents. We note that the tidal current ratios using M_2 as the normalization constituent (i. e. S_2/M_2 , N_2/M_2 ...) at BI4 scale very well ($r^2 = 0.92$) with the alongshore sea level gradient using tidal constants from Broughton Island (67.56°N , 64.02°W) and Cape Dyer (66.58°N , 61.62°W). The tidal current at C_1 is clearly dominated by M_2 with a magnitude of 0.2 m s^{-1} , which is stronger than those of K_1 and S_2 by about 0.1 m s^{-1} , and N_2 and O_1 by 0.05 m s^{-1} . Similar to C_1 , M_2 dominates the tidal currents at C_2 . An interesting feature is the vertical distribution of M_2 at this site. The tidal current in the deep layer is stronger than that in the surface layer. As we can see, the M_2 current increases from 0.14 m s^{-1} in the 10-50 m layer to 0.23 m s^{-1} in the 300-500 m layer. A similar distribution can also be seen for the S_2 constituent. Moreover, K_1 at C_2 is weaker than M_2 , but stronger than O_1 , N_2 and S_2 . The M_2 tidal current at C_3 is stronger than those of the other constituents by 3~10 times. The magnitude of M_2 is comparable to that of C_2 , but the vertical distribution is opposite. On average, the currents for the 5 tidal constituents at C_4 are slightly weaker than those at C_3 except for S_2 , whose magnitude is stronger than that at C_3 by 60%. Compared to C_4 , the 5 tidal components at C_5 and C_6 have a similar vertical distribution but with smaller magnitudes. At WG1, the magnitudes of M_2 and K_1 are comparable and clearly stronger than the other constituents. For M_2 , the magnitude decreases from the surface to the deep layer. On the other hand, the current in deep layer is stronger than that in the surface layer for K_1 . Similarly, the dominant tides at WG3 are M_2 and K_1 , the magnitudes are stronger than those at WG1. As at BI4, the tidal current ratios at WG1 and WG4 scale very well with those derived from alongshore coastal sea level gradients estimated from tidal constants at Rifkol (67.95°N , 53.81°W) and Sisimiut (66.95°N , 53.73°W).

In summary, tidal currents for Davis Strait are strong relative to the mean residual currents, and cannot be ignored in the extreme current analysis. The magnitudes of tidal currents in coastal waters (BI4, WG1 and WG3) are stronger than those in the central Strait (C_1 - C_6). The M_2 constituent in general dominates the tidal currents except at BI4 and WG3, where the magnitudes of K_1 are comparable to or even stronger than those of M_2 .

4.0 Maximum currents

The maximum observed currents including tidal and non-tidal components at each mooring site are shown in Figure 5. Maximum speeds across the Strait mainly occur in the upper layer on Baffin Island shelf, where they reach 2.0 m s^{-1} . The magnitude of the speed is about 1.6 m s^{-1} over the shelf break of West Greenland and the 1.4 m s^{-1} for the central Strait. In the deep layer of the central Strait, the magnitude of the maximum speed is about 0.6 m s^{-1} . The maximum speeds of the tidal current are plotted in Figure 6. These maximum speeds have a similar spatial distribution to that shown in Figure 5, namely, stronger speeds in the coastal/shelf areas and weaker speeds in the deeper region. The maximum tidal speed reaches 0.75 m s^{-1} in the coastal waters, 0.3 m s^{-1} in the central Strait.

5.0 Extreme Currents

Marine operators require information on extreme currents which must include both the tidal and non-tidal flows described above. Extreme currents are commonly reported in terms of statistical probability, for example, the maximum current that is expected over a specified number of years (the return period). As discussed above, the tidal contributions to the total velocity are substantial across Davis Strait, especially at the coastal/shelf sites. For example, the maximum tidal speed is about 50% of the non-tidal component at BI4, and >100% at WG3. Therefore, the tidal speed cannot be ignored in the extreme current analysis. A methodology for statistically combining the non-tidal (residual) and tidal current maxima is therefore required.

5.1 Method

To include the tidal component in the extreme current analysis, a technique called the joint probability method (JPM) is commonly used for estimating the extreme currents (for example, Pugh 1982; Carter et al. 1987; Robinson and Tawn 1997; Jonathan et al. 2012). In the JPM approach, the probability of the total speed at a return period is estimated for the tidal and non-tidal components using joint probability density functions, which are derived from the time series of the observed tidal and non-tidal velocities. Compared to the Generalized Extreme Value methods (GEV), which usually require long time period observations, JMP requires much less data (Pugh 1982). In this report, an alternative approach, based on a Monte Carlo algorithm, is used to account for the tidal and non-tidal components following Oliver et al. (2012). This approach is found to be equivalent to the JPM (Oliver et al., 2012). The time series of tidal current are repeated 10 times ($M=10$) with random start-time and then added to the non-tidal currents. For example, we have:

$$u = u^{NT} + u^T \quad (1)$$

$$v = v^{NT} + v^T \quad (2)$$

where u and v are the time dependent velocities in east and north direction, respectively. The superscripts NT and T stand for the non-tidal and tidal components. Since the time period of the moored data is 7 years, after applying the Monte Carlo technique, the length of the fabricated time series is 70 years. The current speeds are calculated according to

$$|\mathbf{u}| = \sqrt{u^2 + v^2} \quad (3)$$

To estimate the extreme current speed, a Gumbel distribution introduced in Murphy and Jackson (1997), is used. Here only the main part of the method is presented. The steps are as follows:

1. Define the observed annual maximum current speed from Equation 3.

$$U = U_1, U_2, \dots, U_i, \dots, U_N \quad (N = 70) \quad (4)$$

2. Rank the annual maxima by increasing speed, and calculate the cumulative frequency,

$$C(U_i) = \frac{1}{N+1} \quad N = 1, 2, \dots, i \dots 70 \quad (5)$$

3. Determine return periods

$$T(U_i) = \frac{1}{1 - C(U_i)} \quad (6)$$

4. Build prediction formula (Gumbel distribution) using the U_i and $T(U_i)$ pairs

$$U(T) = U_m - [\ln\{-\ln(1 - 1/T)\}] / g_m \quad (7)$$

In which $U(T)$ is extreme current with return period T (unit is year) and U_m and g_m are parameters estimated with a non-linear least square method. Examples at three different locations (BI4, C3 and WG1) across the Strait are shown in Figure 7. In general, the fitted lines agree well with the observations. However, biases are obvious. For example, the points are systematically high (low) changing to systematically low (high) for BI4 (C3, WG1) in the range of 5 to 25 years. The observations clearly fall outside the 95% confidence limits for nearly all observations beyond 5 years. Clearly this indicates some weakness in the method and leads to inaccuracies in the extreme current predictions; however, for the range considered, the inaccuracy seems to be about 0.1 m s^{-1} .

5.2 Extreme Currents

Using the method introduced above, the extreme currents across Davis Strait have been calculated and plotted in Figure 8 and the specific values for selected vertical layers are listed in Table 15. From west to east, two peaks with high speed can be seen in the surface layer (<20 m). The first occurs at site BI4 with the magnitude of 1.87 m s^{-1} at a return period of 10 years (Fig. 9), and 2.06 m s^{-1} at a 30 year return period (Fig. 10). The second is at site C6, where the magnitude reaches 1.46 m s^{-1} at a 10 year return period and 1.61 m s^{-1} at a 30-year return period. The currents are strongest in the surface layer. In the deep layer (>300m) in the central Strait, the extreme current diminishes to $0.5\text{-}0.7 \text{ m s}^{-1}$.

In addition to the Monte Carlo method presented above, we also calculated extreme current speeds using a simple superposition method, in which the extreme currents are obtained by adding the maximum tidal currents to the extreme non-tidal current estimated from the Gumbel distribution. The results are plotted in Figure 11 and 12. Compared to the results from Monte Carlo method, the extreme speeds from the superposition method show a similar spatial structure across Davis Strait, but higher magnitudes: by about 0.7 m s^{-1} in the surface layer and about 0.1 m s^{-1} in the deep layer. The extreme speeds of the non-tidal component are plotted in Figure 13 and 14. The magnitudes of the speeds are lower than those of the previous two cases since the tidal contributions are not included. The realistic extreme current speeds are likely between the output of the Monte Carlo technique and those of the simple superposition.

6.0 Sea-ice draft

To collect ice draft data, Upward-Looking Sonars (ULS) were installed at selected moorings (Fig.1). The working principle and potential errors of the ULS were discussed by Drucker et al. (2003). Ice thickness is the distance from the upper surface of the ice (generally above the water line) to the lower surface (below the water line). The ULS measures ice draft (the thickness of the ice below the water line) which is less than the thickness by about 8-10%. In this report we consider the ice draft only and do not correct for the total thickness. The available ice draft data are listed in Table 16. In addition to the maximum ice draft, we examine two basic time-averaging methods that give draft estimates at approximately daily temporal resolution. One is the daily mean, and the other is the modal mean, in which the modes from 3-hourly intervals in every 48 hours are averaged. The mode is defined as the peak in a binned distribution of values over 3 hours. In Figure 15-20, the time series of raw data, daily mean and modal mean are plotted. For example, Figure 15A shows the data at 5-minute resolution. The ice starts to form in early November 2005 and disappears by the end of August 2006. For most of the ice season there are occasional ice draft measurements that exceed 15 m. Figure 15B shows the daily averages (with standard deviations) of the 5-minute data. For the calculation of most of the statistics we follow Peterson et al. (2008, 2013) and use the modal mean results (e.g. Fig. 15C). To illustrate the features of the ULS ice draft data we use the ice draft data from C1 for the period November 2005 to September 2006. The daily means better show variability at 10-30 day periods superimposed on a seasonal cycle with typical values between 1 or 2 m draft and maximum daily means approaching 4 m, in good agreement with the results of Tang et al. (2004). The mean modal ice draft (computed from the 48 hour mean value of the modes for each 3-hour segment of 5-minute data) in Fig. 15C has typical values less than 1 m and with occasional drafts in the range 2-3 m. From this we conclude that there is substantial variability in the ice draft as observed by the ULS.

In general, ice draft data show strong spatial variations from the Baffin Island coast (C1) to the west Greenland shelf (C6). From west to east, the ice draft and the length of the ice season clearly decrease. At the same time, the ice draft shows strong annual and inter-annual variations. For example, sea-ice draft in winter and spring is generally thicker than that in fall and summer. In 2006, the mean ice draft at C2 is about 1.2 m (Fig. 16), which is only 50% of the ice draft in 2007 (Fig. 19). Ice draft frequency distributions plotted in Figure 21-23 also illustrate the inter-annual (Fig. 21) and spatial (Fig. 23) variability.

Summaries of the ice draft distributions in different years for the 6 instrumented stations are provided in Tables 16-20. In the analysis, the observed data are divided into five categories according to Wadhams et al. (1985): open water ($h_{ice} = 0$), young ice ($0 < h_{ice} \leq 0.5$ m), first year ice ($0.5 \text{ m} < h_{ice} \leq 2.0$ m), multiyear and deformed first year ($2.0 \text{ m} < h_{ice} \leq 5.0$ m) and heavy deformed ice ($h_{ice} > 5.0$ m). During 2005 - 2006, the frequency of ice-free time at site C1 is 15%, corresponding to 55 days, which is less than 1/5 of the ice time (310 days). The predominant ice type is first-year ice with a 34.7% frequency of occurrence, followed by young ice (28.7%). The deformed ice, including the deformed first year ice and heavily deformed ice, was present 21.5% of the year.

The ice data at C2 are available in two observation periods, 2006-2007 and 2007-2008. During the two years, sea ice properties are clearly different particularly for the deformed first year and heavily deformed ice. The frequencies of open water and first year ice in 2006-2007 are higher than those in 2007-2008 by 7% and 4% respectively, but lower in the multiyear and deformed ice by 8.5% and 3.0% respectively. This means that there is more thin ice in 2006 - 2007, but more thick ice in 2007 - 2008. C4 also has two observation periods of 2006-2007 and 2007-2008. Compared to C2, C4 has more ice-free time and the ice is thinner. More young ice occurs in 2006-2007, but less first-year ice in 2007-2008. There is less variation between the two years than at C2. Ice-free time in 2006 - 2007 is more than six months at C6, where the young ice (< 0.5 m) is the most common ice type. Compared to other sites (C1, C2 and C4), the frequency of young ice is high at C6, but lower for other ice types. From the tables, we can also see a strong seasonal variation for all sites. Sea ice is in general thicker in winter and spring and thinner in summer and fall.

In summary, sea ice is generally dominated by first-year ice across Davis Strait. Sea ice on the Baffin Island coast is in general thicker than that in eastern, deep water region. For the maximum draft, however, the ice draft slightly increases from shallow water (C1 and C2), and reaches a maximum at C4 and then decreases at C6.

7.0 Summary

Ocean current and sea-ice draft sensors collected across Davis Strait are analyzed with an aim to provide environmental information for potential oil and gas exploration and drilling in

Baffin Bay and the Davis Strait region. In the analysis, the time series of the raw current data are decomposed into tidal and non-tidal (residual) components. The currents and the sea ice draft data are analyzed based on various statistical approaches. The following conclusions are drawn:

1. Tidal currents cannot be ignored in the extreme current analysis across Davis Strait, especially in the coastal waters (BI4, WG1 and WG3), where the magnitudes of tidal currents are comparable to those of non-tidal flows.
2. The tidal currents across Davis Strait are in general dominated by the M_2 constituent except in the coastal waters (BI4 and WG3), where the magnitude of K_1 is comparable to or stronger than that of M_2 .
3. The maximum speeds across the Strait mainly occur in the Baffin Island coastal area and generally in the fall.
4. The magnitudes of the surface extreme currents near the Baffin Island coast reach $1.9\text{-}2.6\text{ m s}^{-1}$ with a return period of 10 years. In west Greenland region, the surface extreme current speed reaches $1.5\text{-}1.9\text{ m s}^{-1}$ with a 10-year return. In the deep layer ($>300\text{m}$) in the central Strait, the extreme current is typically in the range $0.5\text{ to }0.7\text{ m s}^{-1}$.
5. Sea ice is generally dominated by first-year ice in the Davis Strait area. The sea ice draft on the Baffin Island shelf is generally thicker than in the deep water region to the east. Sea ice is generally thicker in winter and spring than in summer and fall. Mean ice draft is $1.4\text{ m } (\pm 1.9\text{m})$ at Baffin Island Shelf and $0.2\text{ m } (\pm 0.4\text{m})$ at the west Greenland Shelf. The maximum ice drafts across the Strait from all of the data were surprisingly uniform at 18.4 , 19.4 , 20.8 and 17.3 m for C1, C2, C4, and C6 respectively.

8.0 ACKNOWLEDGMENTS

The publication of the report is supported by the Program of Energy Research and Development (PERD). The Davis Strait study is part of U.S. National Science Foundation Freshwater Initiative (2004-2007) and the International Polar Year (IPY) and Arctic Observing Network (AON) (2007-2010) programs under grants OPP0230381, ARC0632231 and ARC1022472. We thank E. Oliver (University of Tasmania) for providing Matlab program code of Monte Carlo technique. We also thank Jim Hamilton and Adam Drozdowski for their helpful reviews of an early version of the report.

9.0 References

- Canadian Ice Service, 2012. Sea Ice Climatic Atlas for Northern Canadian Waters 1981-2010. Available on-line at <http://www.ec.gc.ca/glaces-ice/>.
- Carter, D.J.T., Loynes, J., and Challenor, P.G. 1987. Estimation of extreme current speeds over the continental slope of Scotland. Report 239. Institute of Oceanographic Sciences, Wormley. pp20.
- Crane, R.G. 1978. Seasonal variations of sea ice extent in the Davis Strait-Labrador Sea area and relationships with synoptic scale atmospheric circulation. *Arctic*, 31, 434-447.
- Cuny, J., Rhine, P., and Kwok, R. 2005. Davis Strait volume, freshwater and heat fluxes. *Deep-Sea Res. I* 52(3): 519–542.
- Curry, B., Lee, C.M., and Petrie, B. 2011. Volume, freshwater, and heat fluxes through Davis Strait, 2004-2005. *J. Phys. Oceanogr.* 41: 429-436.
- Drucker, R., Martin, S., and Moritz, R. 2003. Observations of ice thickness and frazil ice in the St. Lawrence Island polynya from satellite imagery, upward looking sonar, and salinity/temperature moorings. *J. Geophys. Res.*, 108(C5), 3149, doi:10.1029/2001JC001213.
- Jonathan, P., Ewans, K., and Flynn, J. 2012. Joint modelling of vertical profiles of large ocean currents. *Ocean Engineering* 42: 195-204.
- Murphy, B., and Jackson, P.L. 1997. Extreme Value Analysis: Return Periods of Severe Wind Events in the Central Interior of British Columbia. MacGregor Model Forest Association, Prince George, BC. 38pp.
- Oliver, E.C., Sheng, J., Thompson, K.R., Urrego Blanco, J.R. 2012. Extreme surface and near-bottom currents in the northwest Atlantic. *Nat. Hazards.*, DOI 10.1007/s11069-012-0303-5.
- Pawlowicz, R., Beardsley, B., Lentz, S. 2002. Classical tidal harmonic analysis including error estimates in MATLAB using T-TIDE. *Computers and Geosciences* 28: 929-937.
- Peterson, I. K., Prinsenber, S.J., and Holladay, J.S. 2008. Observations of sea ice thickness, surface roughness and ice motion in Amundsen Gulf. *J. Geophys. Res.* 113, C06016, doi:10.1029/2007JC004456.
- Peterson, I.K., Prinsenber, S.J., and Belliveau, D. 2013. Sea-Ice Draft and Velocities from Moorings on the Labrador Shelf (Makkovik Bank): 2003-2011. *Can. Tech. Rep. Hydrogr. Ocean Sci.* 281: v + 32 p.
- Pugh, D.T. 1982. Estimating extreme currents by combining tidal and surge probabilities, *Ocean Engineering* 9: 361-372.
- Robinson, M. E., and Tawn, J.A. 1997. Statistics for extreme sea currents. *Appl. Statist.* 46: 183-205.
- Ross, C.K. 1992. Moored current meter measurements across Davis Strait. NAFO Research Document Technical report 92/70., 8 pp.
- Ross, C.K. 1990a. Current and temperature data from northwestern Baffin Bay, September 1983-September 1984. *Canadian Data Report of Hydrography and Ocean Science* 78, vii + 227 pp.
- Ross, C.K. 1990b. Current and temperature data from southwestern Baffin Bay, October 1984-October 1985. *Canadian Data Report of Hydrography and Ocean Science* 79, vii + 180 pp.
- Ross, C.K. 1991. Current, temperature and salinity data from northern Baffin Bay, October 1985-October 1986. *Canadian Data Report of Hydrography and Ocean Science* 95, vii + 161 pp.

- Ross, C.K. 1993. Current and temperature data from eastern Baffin Bay, October 1986-September 1987. Canadian Data Report of Hydrography and Ocean Science 118, vii +193 pp.
- Tang, C.L., Ross, C.T., Yao, T., Petrie, B., Detracey, B.D., and Dunlap, E. 2004. The circulation, water masses and sea-ice of Baffin Bay. *Prog. Oceanogr.* 63: 183-228.
- Wadhams, P., McLaren, A.S., and Weintraub, R. 1985. Ice thickness in Davis Strait in February from submarine sonar profiles. *J. Geophys. Res.* 90: 1069-1077.
- Wu, Y., Tang, C.L., and Hannah, C.G. 2012. Circulation in eastern Canadian seas. *Prog. Oceanogr.* 106: 28-48.

Table 1 Mooring information, 2004-2011. An × indicates no data available, an √ indicates data

Moorings		2004- 2005	2005- 2006	2006- 2007	2007- 2008	2008- 2009	2009- 2010	2010- 2011
ADCP	BI3	√	×	√	×	×	×	×
	BI4	×	√	×	×	√	√	√
	C1	√	√	√	√	√	√	√
	C2	√	√	√	√	√	√	√
	C3	√	√	×	√	√	√	√
	C4	√	×	√	√	√	√	√
	C5	√	√	√	√	√	√	√
	C6	√	×	√	√	√	√	√
	WG1	√	√	√	√	√	√	√
	WG3	√	√	√	√	×	×	×
	WG4	×	×	×	×	√	√	√
	RCM8	C1	√	√	×	√	√	√
C2		√	√	√	√	√	√	√
C3		√	√	×	√	√	√	√
C4		√	√	√	√	√	√	√
C5		√	√	√	√	√	√	√
C6		×	×	√	√	√	√	√

available.

Table 15 Extreme speeds (unit is m s^{-1}) for 10 and 30 year return periods

Mooring		Return period (year)					
		10			30		
Depth (m)		Best estimation	95% confidence		Best estimation	95% confidence	
			Upper	lower		upper	lower
B14	10-20	1.87	1.88	1.86	2.06	2.08	2.05
	20-100	1.54	1.55	1.53	1.70	1.71	1.68
	100-300						
	300-500						
C1	10-20	1.19	1.19	1.18	1.29	1.30	1.28
	20-100	0.95	0.95	0.94	1.02	1.03	1.02
	100-300	0.78	0.78	0.77	0.85	0.86	0.84
	300-500						
C2	10-20	1.19	1.18	1.18	1.31	1.32	1.30
	20-100	0.91	0.91	0.90	1.01	1.02	1.00
	100-300	0.68	0.67	0.67	0.72	0.72	0.72
	300-500	0.68	0.68	0.68	0.74	0.74	0.73
C3	10-20	1.28	1.29	1.27	1.48	1.50	1.46
	20-100	0.81	0.81	0.80	0.90	0.92	0.89
	100-300	0.52	0.52	0.51	0.56	0.57	0.56
	300-500	0.48	0.47	0.47	0.51	0.52	0.51
C4	10-20	1.37	1.38	1.35	1.61	1.64	1.59
	20-100	0.83	0.83	0.82	0.92	0.93	0.91
	100-300	0.56	0.56	0.55	0.61	0.62	0.60
	300-500	0.49	0.49	0.49	0.54	0.55	0.53
C5	10-20	1.40	1.41	1.38	1.62	1.66	1.58
	20-100	0.83	0.83	0.82	0.92	0.94	0.91
	100-300	0.66	0.66	0.65	0.73	0.74	0.72
	300-500	0.58	0.57	0.57	0.63	0.64	0.62
C6	10-20	1.46	1.47	1.43	1.80	1.85	1.76
	20-100	0.84	0.86	0.84	0.97	0.99	0.95
	100-300	0.63	0.63	0.62	0.70	0.72	0.69
	300-500						
WG1	10-20	1.38	1.39	1.37	1.59	1.61	1.58
	20-100	0.95	0.95	0.94	1.03	1.04	1.03
	100-300	0.80	0.81	0.79	0.91	0.93	0.90
	300-500						
WG3	10-20	1.12	1.12	1.12	1.25	1.26	1.24
	20-100	1.05	1.06	1.05	1.19	1.20	1.18
	100-300						
	300-500						

Table 16 Distributions of ice draft over five ranges, and annual and maximum ice draft. The numbers in the brackets are standard deviations.

Moorings		Percentage of ice in draft ranges (%)					Mean draft (m)	Maximum draft (m)
		Open water	0 - 0.5 m	0.5 - 2.0 m	2.0 - 5.0 m	>5.0 m		
2005-2006	C1	15.1	28.7	34.7	15.7	5.8	1.36 (1.92)	18.4
	C2	38.1	23.7	27.9	7.9	2.4	0.8 (1.4)	19.4
2006-2007	C4	43.5	24.1	29.8	2.3	0.3	0.4 (0.7)	20.6
	C6	55.9	29.4	14.2	0.4	0.0	0.2 (0.4)	17.3
2007-2008	C2	31.0	23.2	23.8	16.5	5.5	1.2 (1.9)	19.2
	C4	43.8	21.8	32.0	2.1	0.3	0.4 (0.7)	20.8

Table 17 Distributions of ice draft over five ranges, and annual and maximum ice draft in October-December. The numbers in the brackets are standard deviations.

Moorings		Percentage of ice in draft ranges (%)					Mean draft (m)	Maximum draft (m)
		Open water	0 - 0.5 m	0.5 - 2.0 m	2.0 - 5.0 m	>5.0 m		
2005-2006	C1	6.4	47.8	38.1	6.8	0.9	0.7 (1.0)	17.1
	C2	59.3	35.9	4.2	0.4	0.1	0.1 (0.4)	18.8
2006-2007	C4	71.8	22.9	5.2	0.0	0.0	0.1 (0.3)	18.8
	C6	90.9	8.8	0.3	0.0	0.0	0.0 (0.1)	1.1
2007-2008	C2	34.8	34.3	25.3	4.9	0.8	0.5 (0.9)	15.6
	C4	70.5	21.1	7.9	0.4	0.1	0.1 (0.4)	18.2

Table 18 Distributions of ice draft over five ranges, and annual and maximum ice draft in January-March. The numbers in the brackets are standard deviations.

Moorings		Percentage of ice in draft ranges (%)					Mean draft (m)	Maximum draft (m)
		Open water	0 - 0.5 m	0.5 - 2.0 m	2.0 - 5.0 m	>5.0 m		
2005-2006	C1	4.1	24.6	37.5	24.2	9.5	1.9 (2.2)	17.5
	C2	4.4	33.2	51.8	8.8	1.8	1.0 (1.2)	19.4
2006-2007	C4	4.2	41.2	51.7	2.6	0.3	0.6 (0.7)	20.4
	C6	11.0	61.0	27.2	0.7	0.1	0.4 (0.4)	17.1
2007-2008	C2	0.7	21.1	37.9	30.4	9.9	2.1 (2.0)	15.8
	C4	3.6	35.0	57.4	3.6	0.4	0.7 (0.7)	9.80

Table 19 Distributions of ice draft over five ranges, and annual and maximum ice draft in April-June. The numbers in the brackets are standard deviations.

Moorings		Percentage of ice in draft ranges (%)					Mean draft (m)	Maximum draft (m)
		Open water	0 - 0.5 m	0.5 - 2.0 m	2.0 - 5.0 m	>5.0 m		
2005-2006	C1	14.2	18.9	40.0	19.1	7.8	1.7 (2.1)	18.4
	C2	22.0	19.2	38.0	15.2	5.6	1.4 (2.0)	19.3
2006-2007	C4	16.3	22.5	55.5	5.0	0.7	0.8 (0.9)	20.6
	C6	32.0	41.4	25.7	0.8	0.1	0.3 (0.5)	17.3
2007-2008	C2	19.8	21.3	25.6	24.3	9.0	1.8 (2.2)	19.2
	C4	21.3	24.8	49.8	3.5	0.7	0.7 (0.9)	20.8

Table 20 Distributions of ice draft over five ranges, and annual and maximum ice draft in July-September. The numbers in the brackets are standard deviations.

Moorings		Percentage of ice in draft ranges (%)					Mean draft (m)	Maximum draft (m)
		Open water	0 - 0.5 m	0.5 - 2.0 m	2.0 - 5.0 m	>5.0 m		
2005-2006	C1	44.3	32.4	17.0	4.8	1.5	0.5 (1.1)	17.2
	C2	78.6	4.2	10.2	5.3	1.6	0.4 (1.3)	19.0
2006-2007	C4	84.0	10.1	4.4	1.2	0.3	0.1 (0.6)	19.7
	C6	99.6	0.4	0.0	0.0	0.0	0.0 (0.0)	2.9
2007-2008	C2	83.2	15.9	0.7	0.0	0.1	0.0 (0.4)	18.9
	C4	100.0	0.0	0.0	0.0	0.0	0.0 (0.0)	0.0

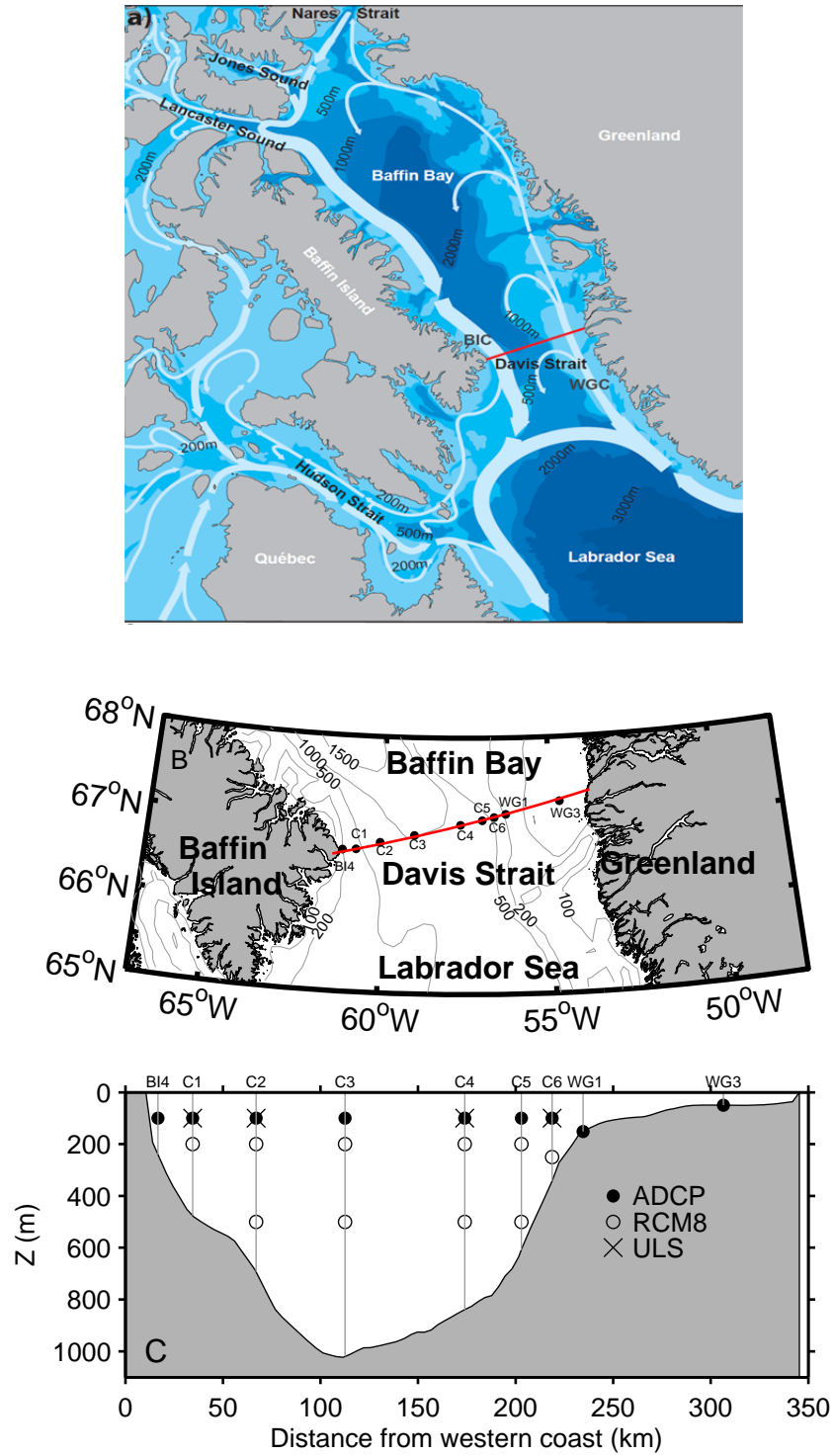


Fig. 1 General circulation (A) and horizontal (B) and vertical (C) arrangement of the moored array used for sea ice and velocity analysis.

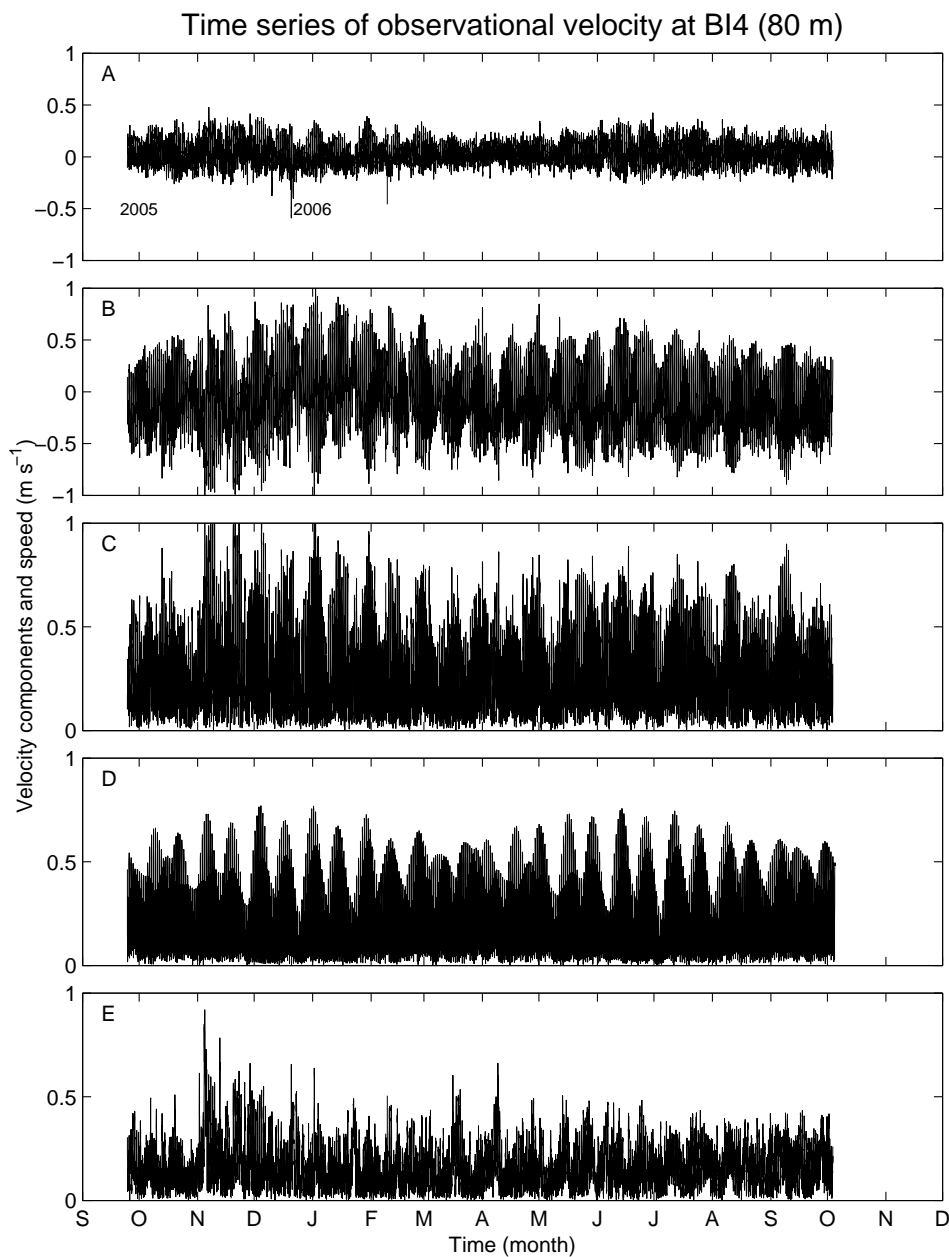


Fig. 2 An example of time series velocity at B14 in 2005-2006. Panels A - E indicate east-west velocity u ; north-south velocity v ; total speed; tidal flow speed and residual flow speed, respectively.

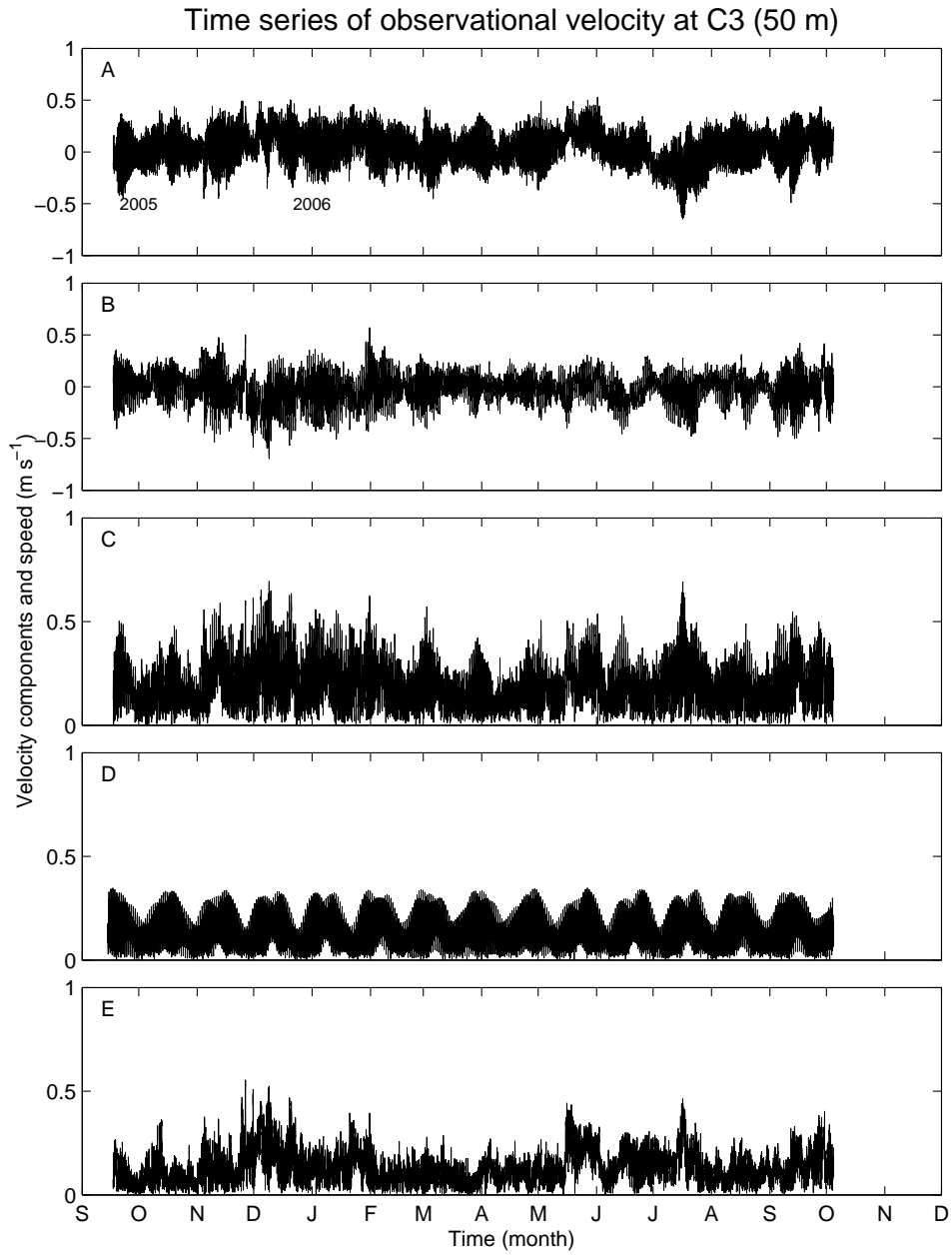


Fig. 3 An example of time series velocity at C3 in 2005-2006. Panels A - E indicate total velocity u ; total velocity v ; total speed; tidal flow speed and residual flow speed, respectively.

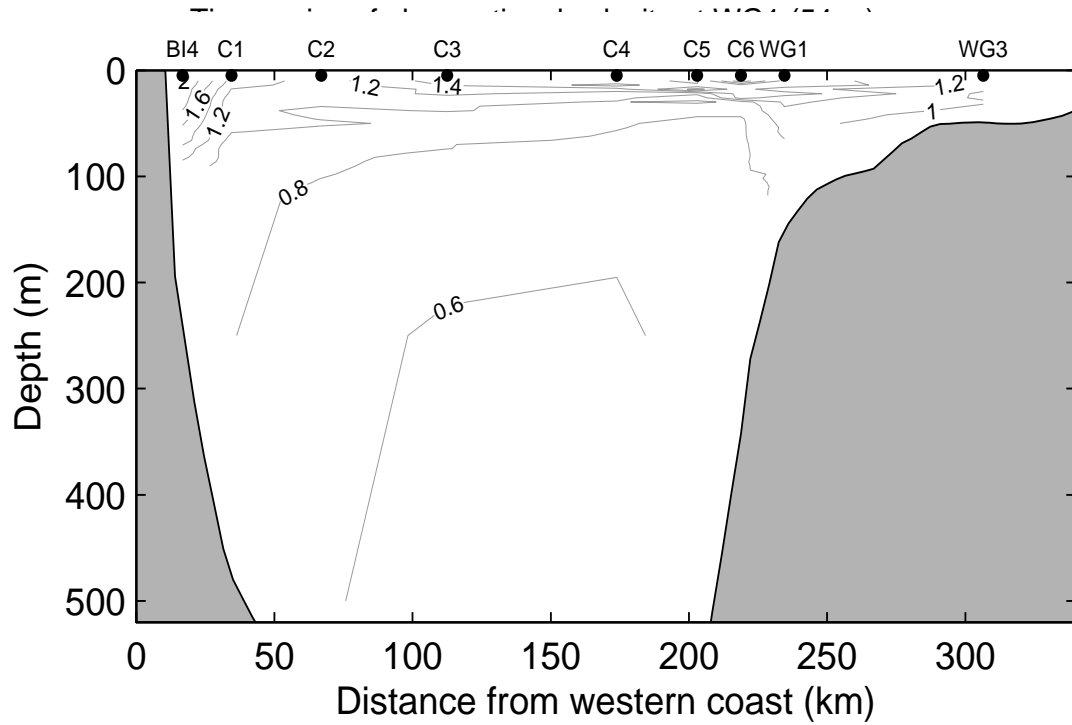


Fig. 5 Maximum observed speeds for the 2004-2010 period.

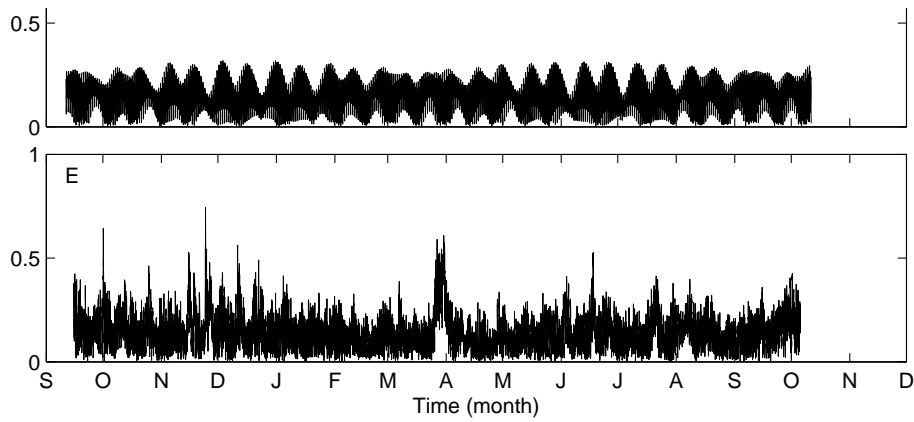


Fig. 4 An example of time series velocity at WG1 in 2005-2006. Panels A - E indicate total velocity u ; total velocity v ; total speed; tidal flow speed and residual flow speed, respectively.

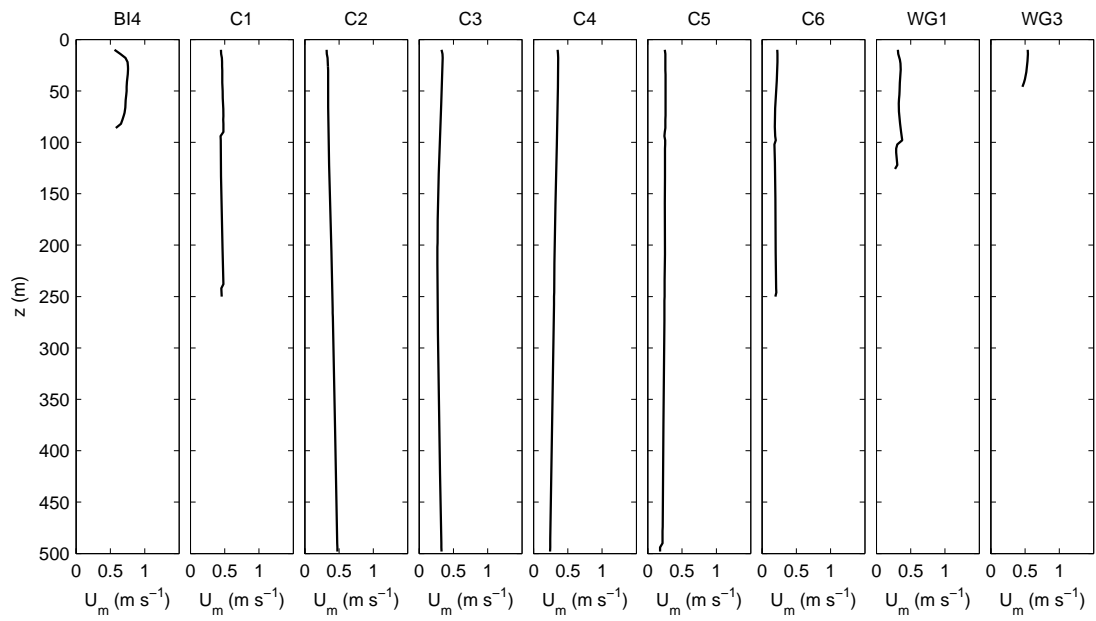


Fig. 6 Vertical profiles of the maximum observed tidal speed.

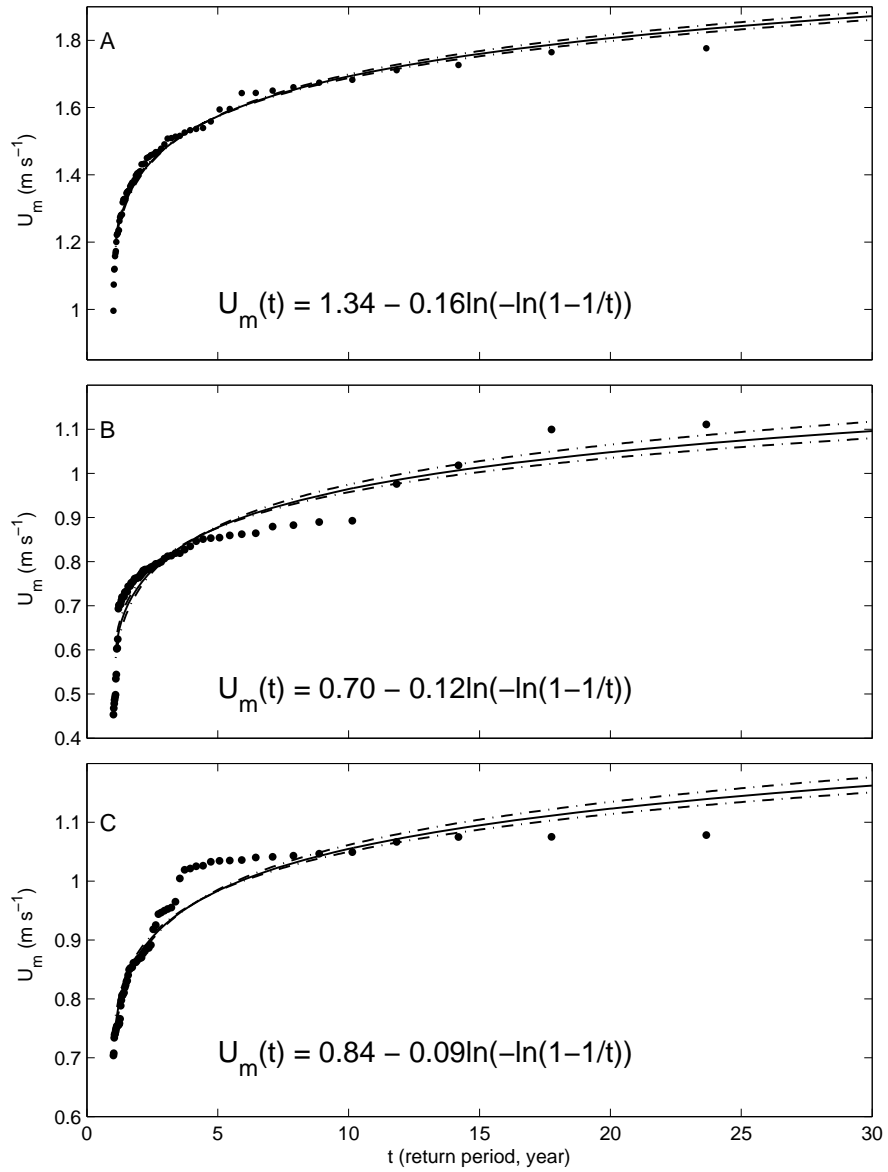


Fig. 7 Examples of Gumbel distribution at BI4 (30m) (A), C3 (30m) B, and WG1 (30m) (C). In each panel, dots indicate the observations (from JPM), solid black line represents the fitted curve, and the dash-dot lines are the 95% confidence limits.

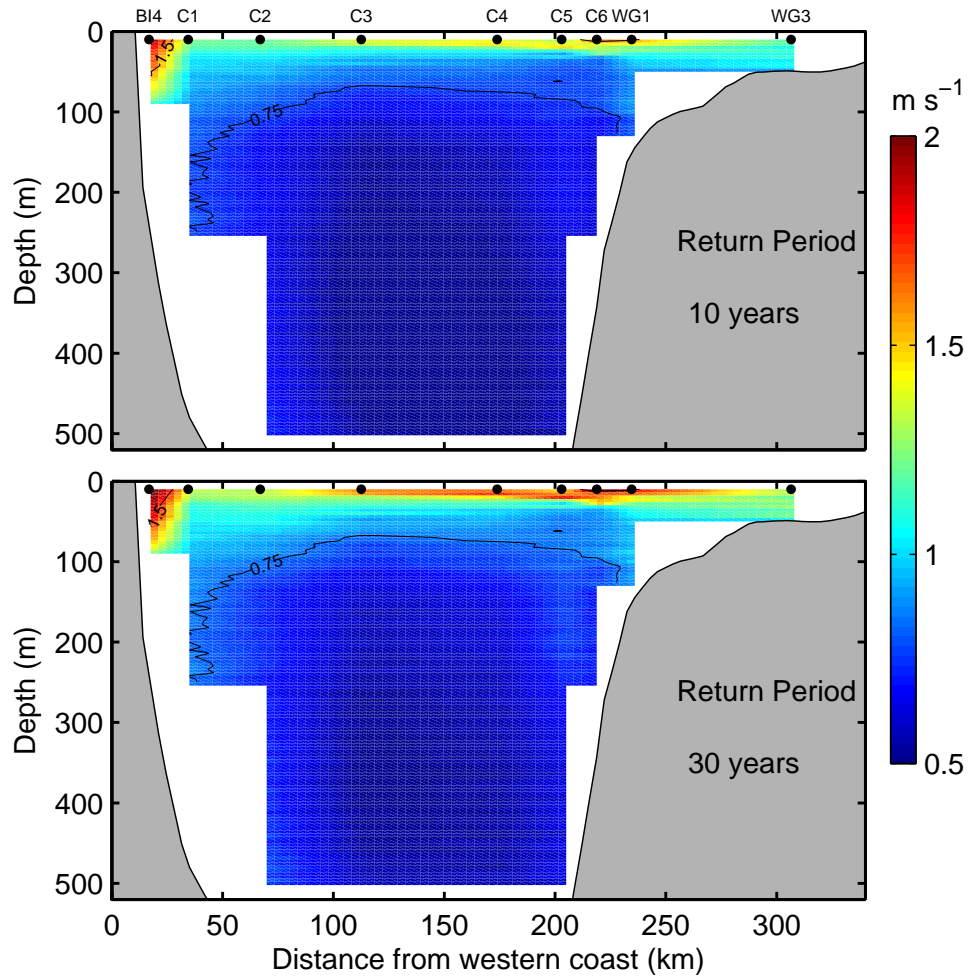


Fig. 8 Extreme speeds for 10- and 30- year return periods with JPM method.

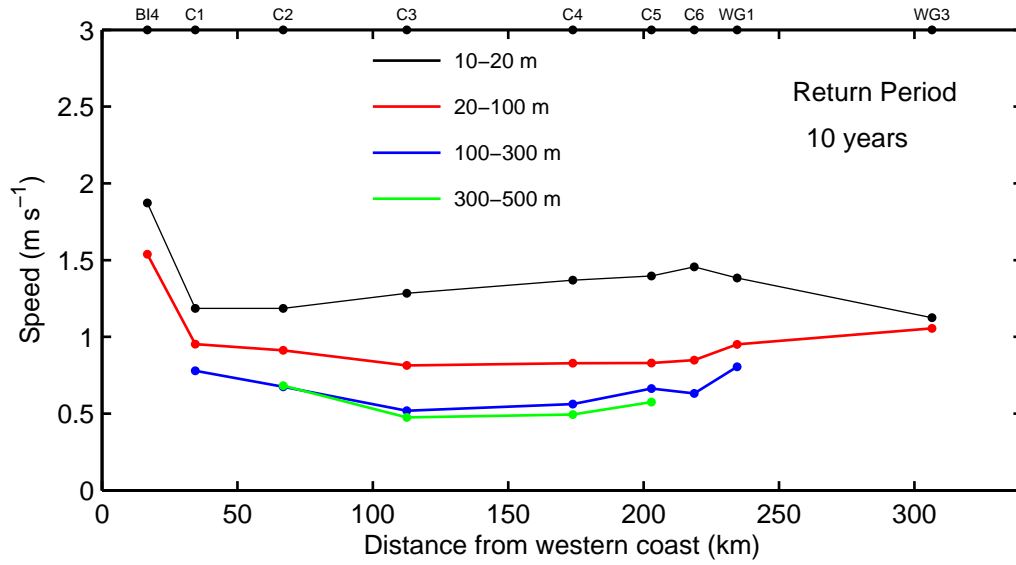


Fig. 9 Extreme speeds at selected layers for 10-year return period with JPM method.

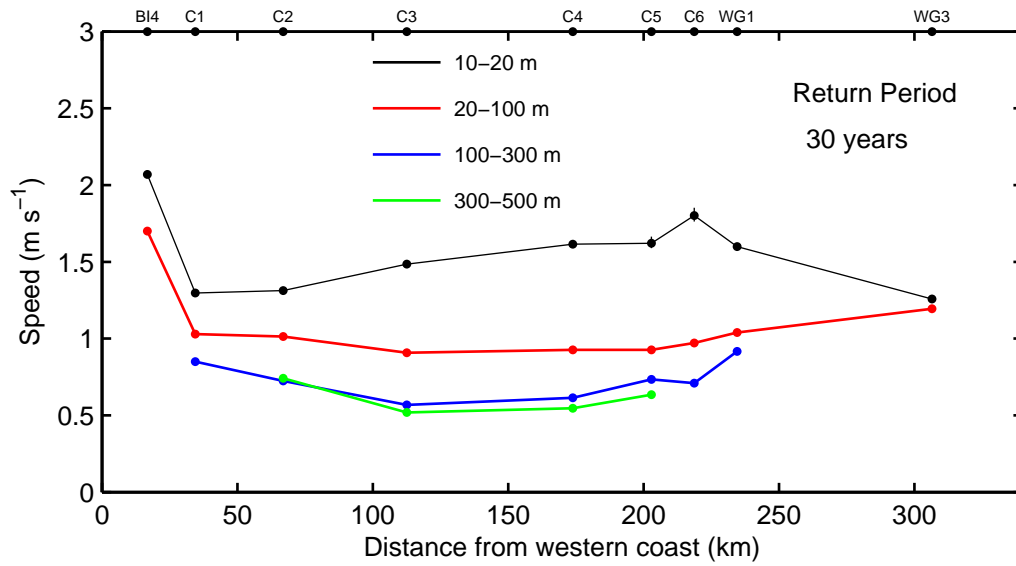


Fig. 10 Extreme speeds at selected layers, for 30-year return period with JPM method.

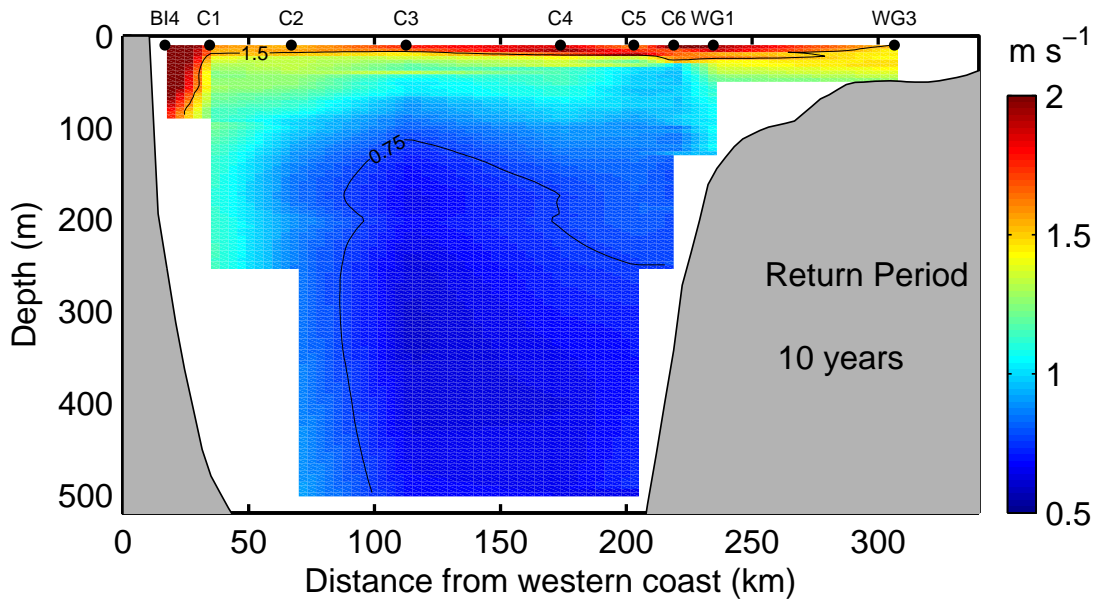


Fig. 11 Extreme speeds for 10-year return period using the simple superposition method.

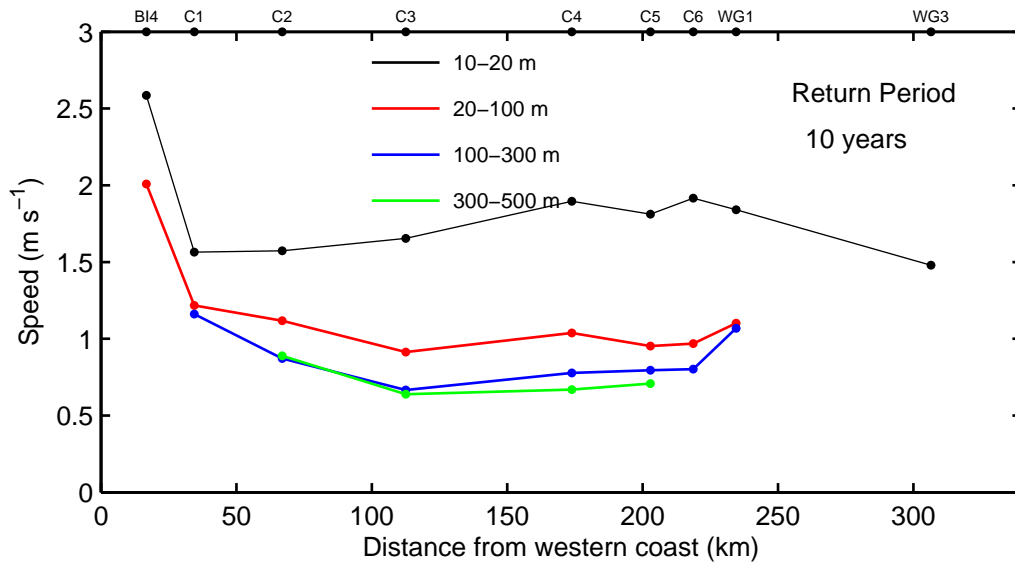


Fig. 12 Extreme speeds at selected layers for 10-year return period using the direct superposition method.

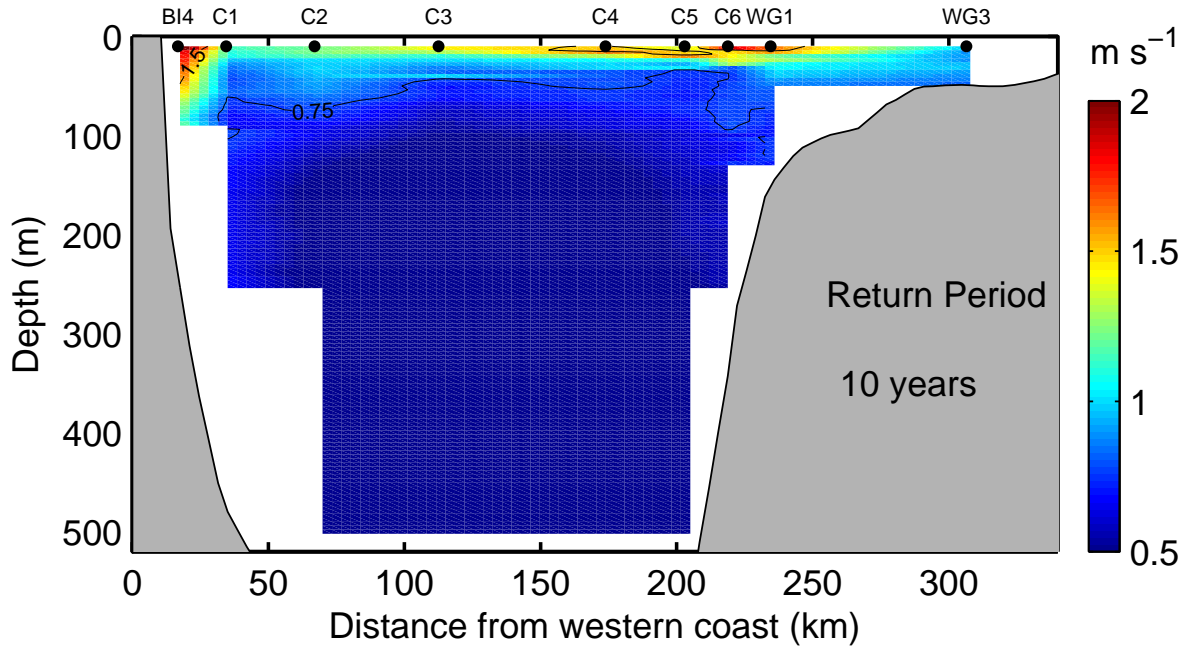


Fig. 13 Extreme non-tidal speeds at selected depths for 10-year return period.

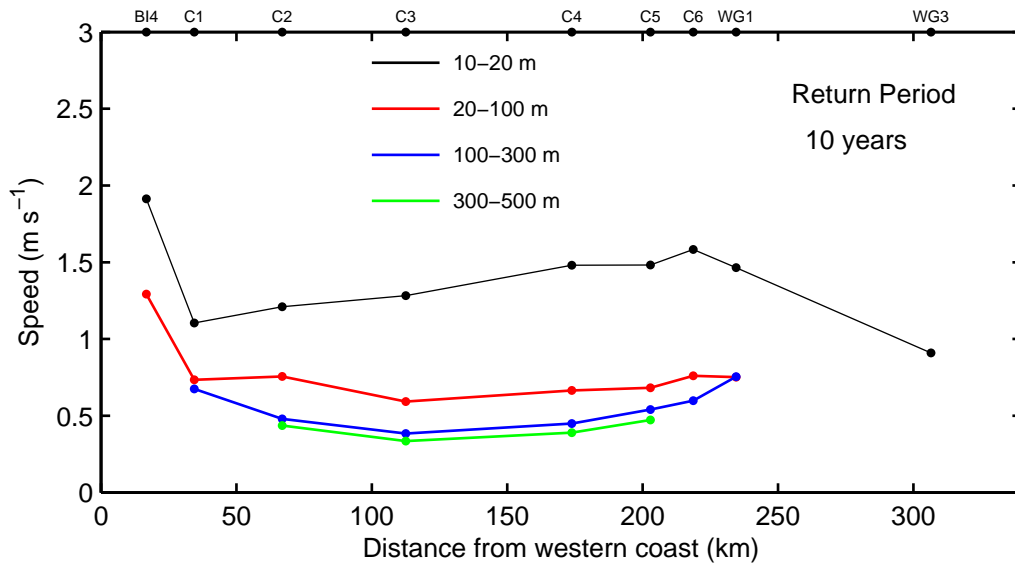


Fig. 14 Extreme non-tidal speeds at selected layers for 10-year return.

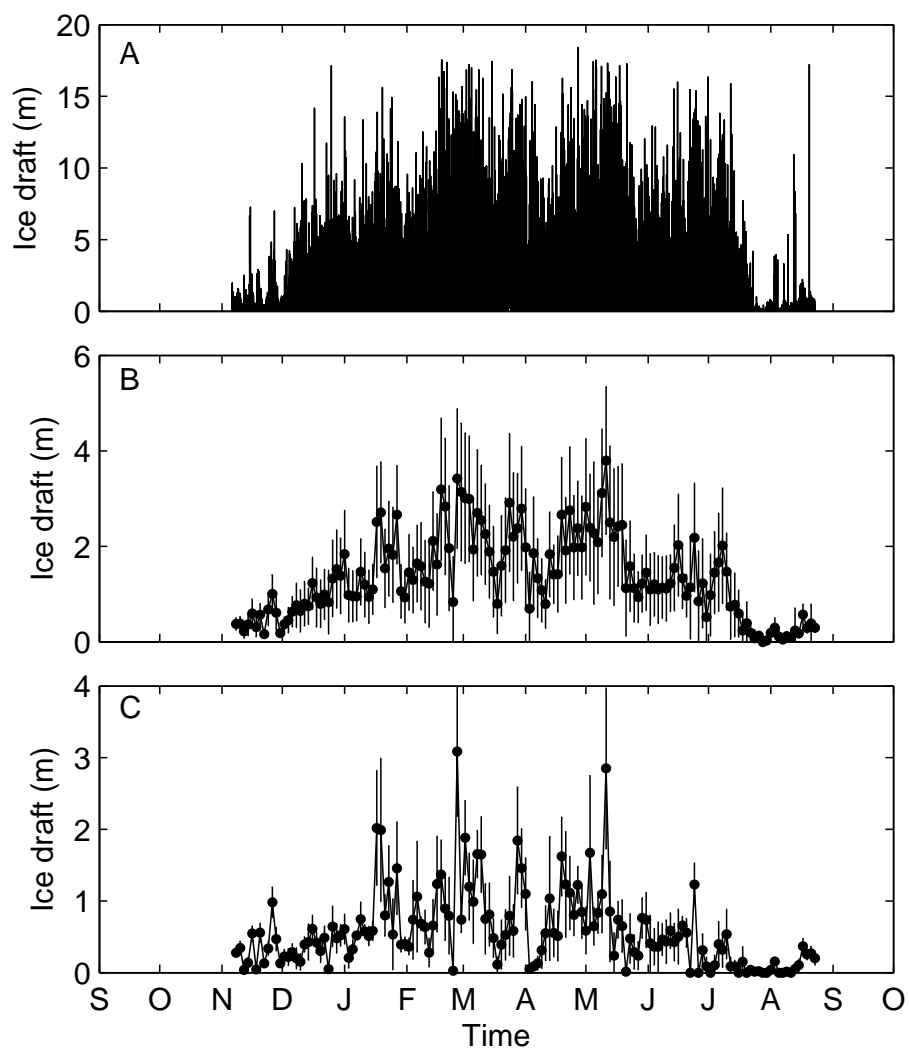


Fig. 15 Time series of ice draft at C1 in 2005 - 2006. A: raw data, B: daily mean and C: mean of the daily modal.

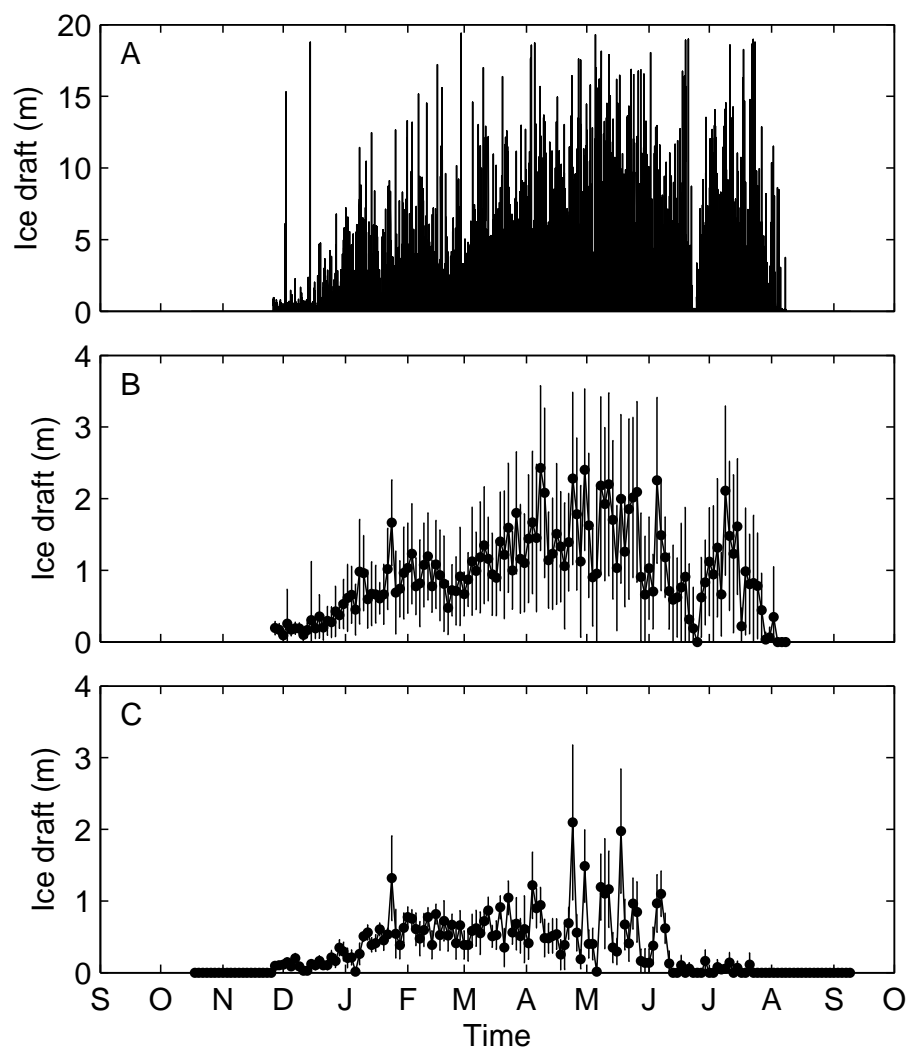


Fig. 16 Time series of ice draft at C2 in 2006 - 2007. A: raw data, B: daily mean and C: mean of the daily modal

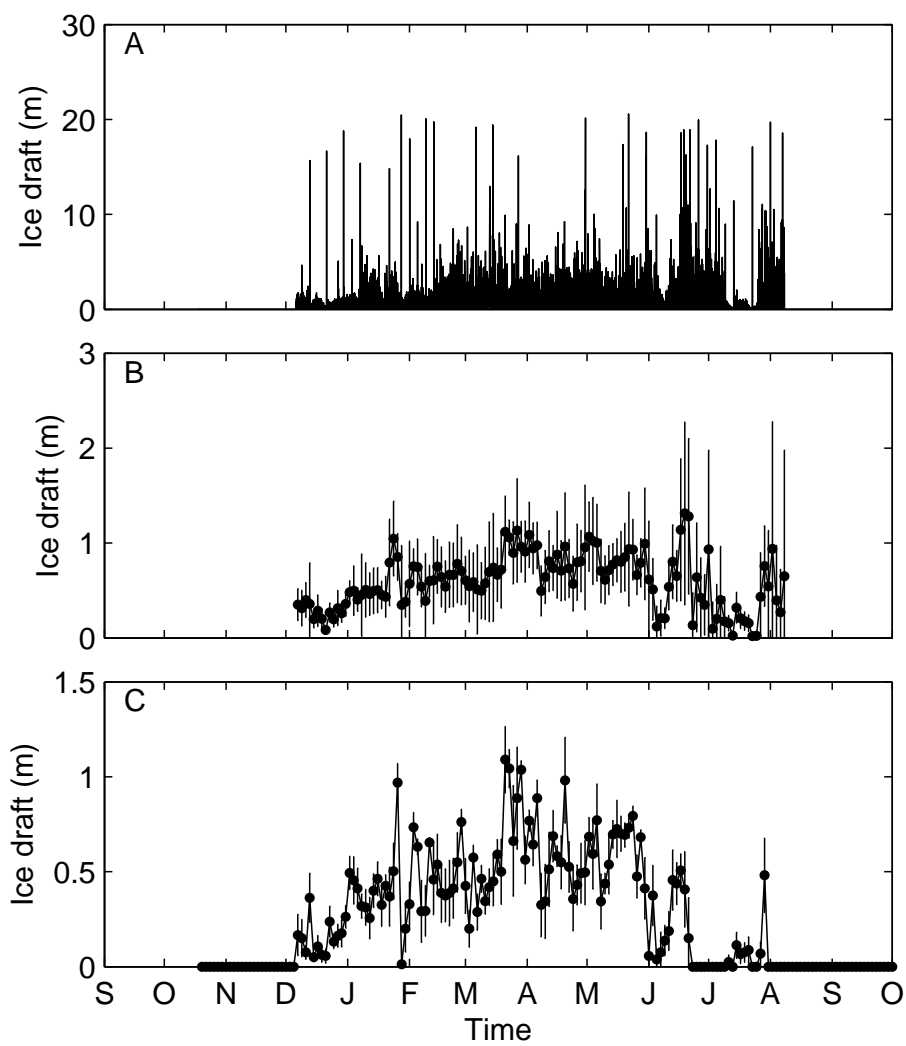


Fig. 17 Time series of ice draft at C4 in 2006 - 2007. A: raw data, B: daily mean and C: mean of the daily modal

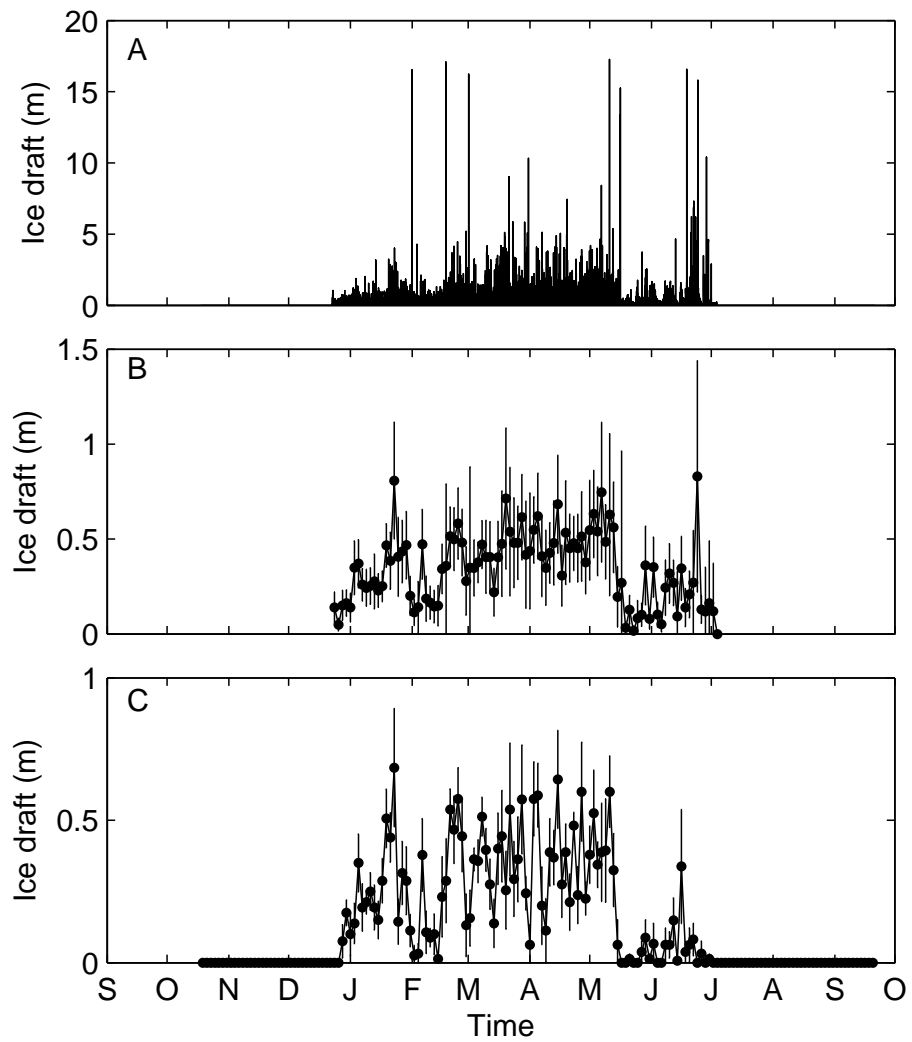


Fig. 18 Time series of ice draft at C6 in 2006 - 2007. A: raw data, B: daily mean and C: mean of the daily modal

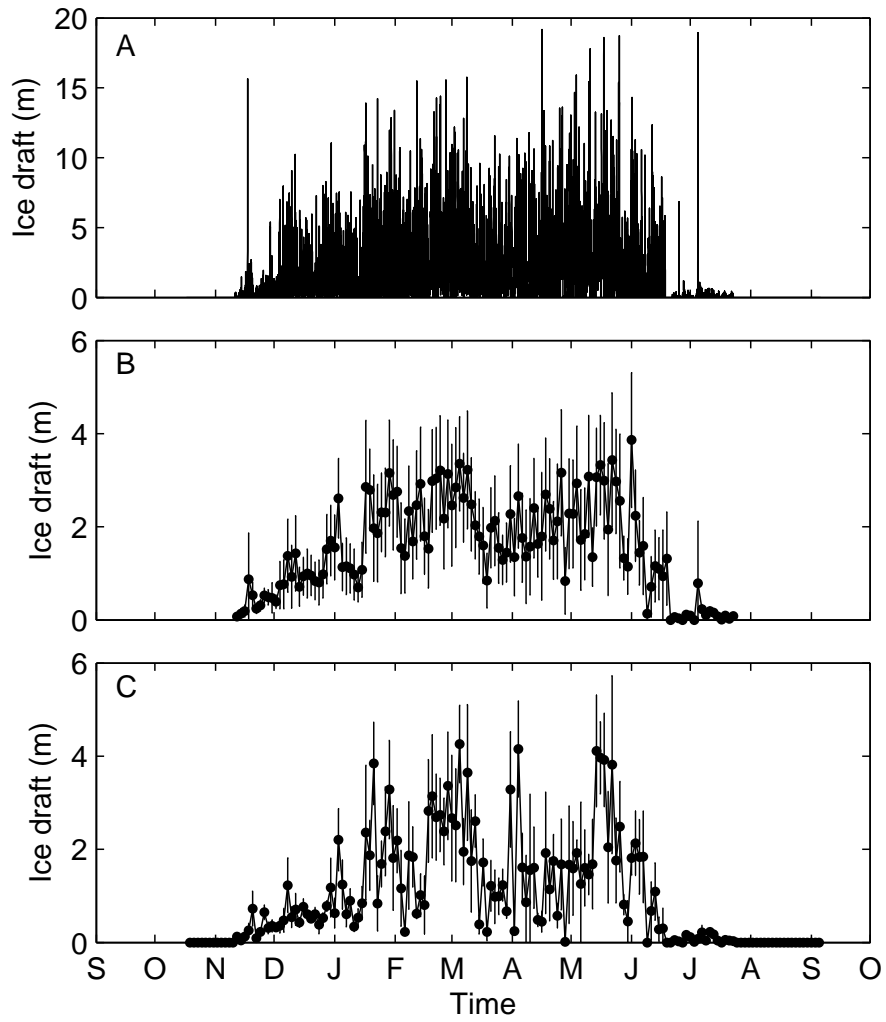


Fig. 19 Time series of ice draft at C2 in 2007 - 2008. A: raw data, B: daily mean and C: mean of the daily modal

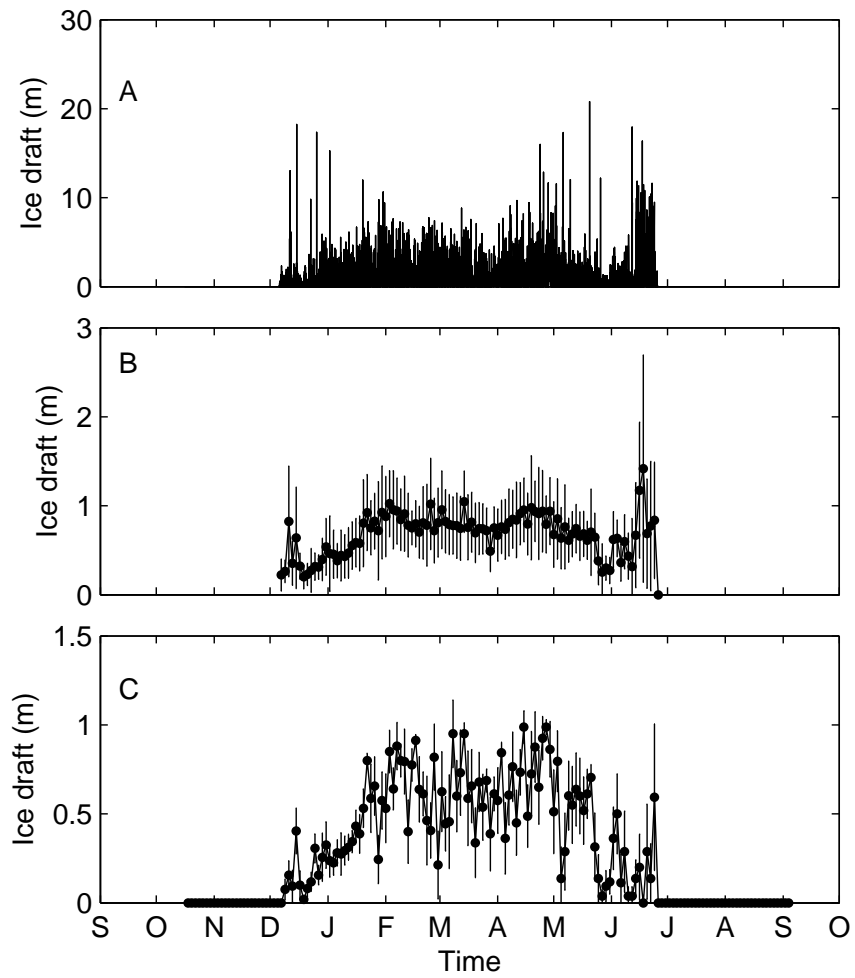


Fig. 20 Time series of ice draft at C4 in 2007 - 2008. A: raw data, B: daily mean and C: mean of the daily modal

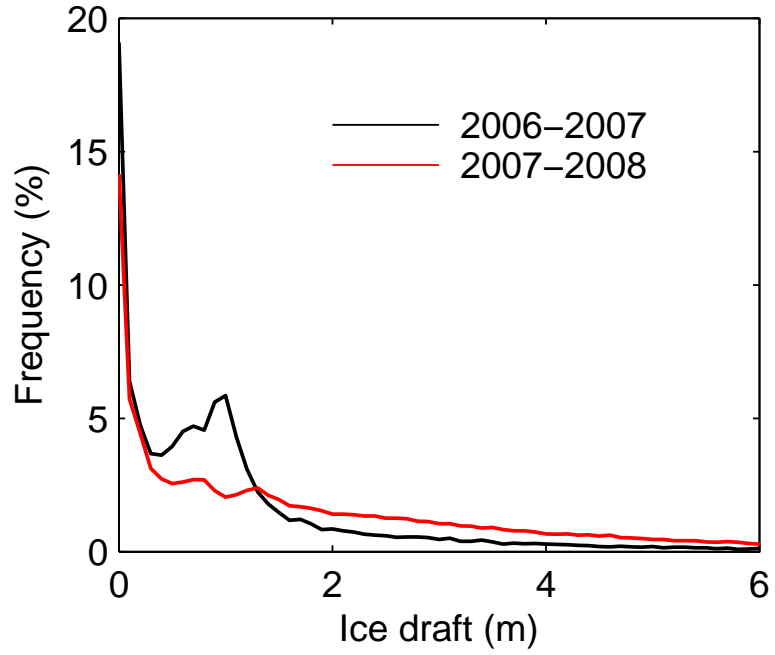


Fig. 21 Ice draft frequency distribution at C2

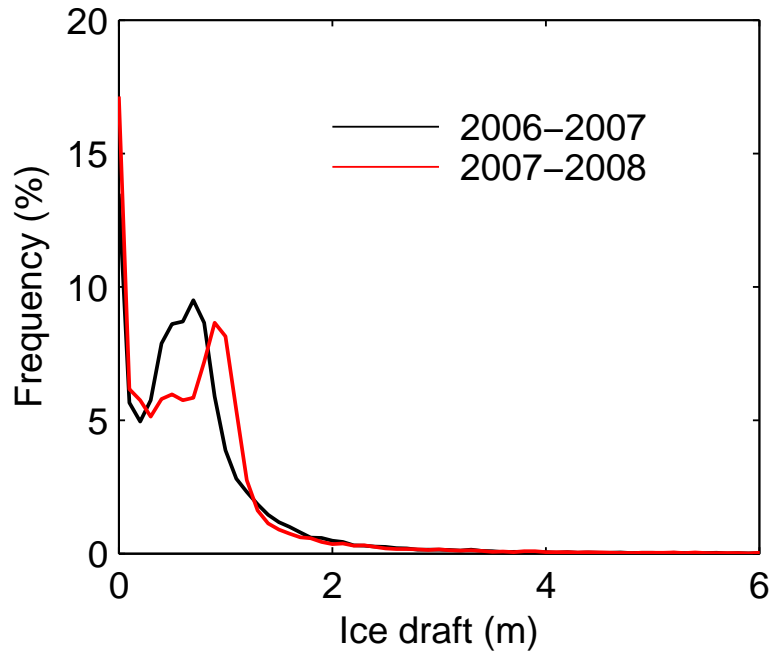


Fig. 22 Ice draft frequency distribution at C4

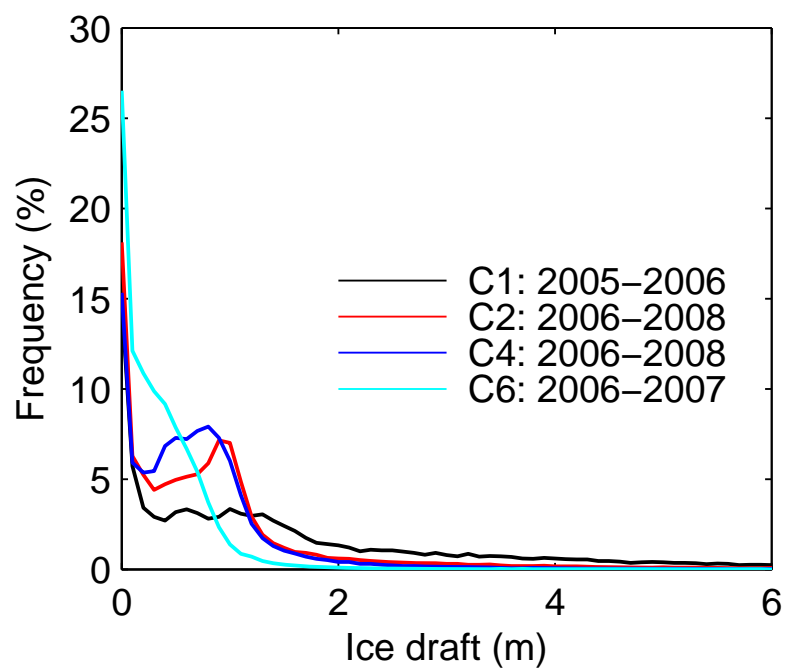


Fig. 23 Ice draft frequency distributions at C1, C2, C4 and C6.